Random local strain effects in the relaxor ferroelectric BaTi1-xZrxO3: experimental and theoretical investigation

Claire Laulhé, Francoise Hippert, Jens Kreisel, Alain Pasturel, Annie Simon, Jean-Louis F Hazemann, Robert Bellissent, Gabriel Cuello

Random local strain effects in the relaxor ferroelectric $BaTi_{1-x}Zr_xO_3$: experimental and theoretical investigation

C. Laulhé[ab]*, F. Hippert[a], J. Kreisel[a], A. Pasturel[c], A. Simon[d], J.-L. Hazemann[e], R. Bellissent[f] and G.J. Cuello[g]

[a]*Laboratoire des Matériaux et du Génie Physique (CNRS – Grenoble INP), MINATEC, 3 Parvis Louis Néel, B.P. 257, F-38016 Grenoble Cedex 01, France;* [b]*Synchrotron SOLEIL, L'Orme des Merisiers, Saint Aubin – B.P. 48, F-91192 Gif-sur-Yvette Cedex, France;* [c]*Laboratoire Science et Ingénierie des MAtériaux et Procédés, 1130 rue de la Piscine, BP 75, F-38402 Saint Martin d'Hères Cedex, France;* [d]*CNRS, Université de Bordeaux, ICMCB, 87 avenue A. Schweitzer, F-33608 PESSAC, Grenoble, France;* [e]*Laboratoire de Cristallographie (CNRS), 25 rue des Martyrs, BP 166, F-38042 Grenoble Cedex 9, France;* [f]*CEA Grenoble, INAC/SPSMS, 17 rue des Martyrs, F-38054 Grenoble Cedex 9, France;* [g]*Institut Laue-Langevin, 6 rue Jules Horowitz, B.P.156, F-38042 Grenoble Cedex 9, France*

We report an investigation of the local structure in homovalent-substituted $BaTi_{1-x}Zr_xO_3$ relaxors by a combination of experimental and theoretical methods, namely neutron total scattering, X-ray absorption spectroscopy, and supercell *ab-initio* calculations. It is shown that unlike Zr atoms, Ti atoms are largely displaced in their octahedra, and are thus associated with strong local dipole moments. Besides, we give evidence that the difference in the size of Ti^{4+} and Zr^{4+} cations leads to a significant size mismatch of the Ti–O_6 and Zr–O_6 octahedra. When they link to form the perovskite structure of $BaTi_{1-x}Zr_xO_3$, the O_6 octahedra undergo slight distortions in order to accommodate their different sizes. It is shown that they are compressed in the direction of Zr neighbors, and expanded in the direction of Ti neighbors. The polar Ti displacements, which are sensitive to the octahedral distortions, then become constrained in their orientation according to the local Zr/Ti distribution. Such constraints impede a perfect alignment of all the Ti displacements as existing in the classic ferroelectric $BaTiO_3$. Our results shed light on the structural mechanisms that lead to disordered Ti displacements in $BaTi_{1-x}Zr_xO_3$ relaxors, and probably in other $BaTiO_3$-based relaxors with homovalent substitution.

Keywords: ferroelectrics; relaxor ferroelectrics; local structure; pair distribution function; X-ray absorption spectroscopy; supercell *ab-initio* calculations

1. Introduction

Relaxors form a fascinating class of materials which exhibit complex structural and dynamical behaviors on multiple time and length scales [1], with important technological applications such as capacitors and piezoelectric devices [2]. They are characterized by a broad and frequency-dependent maximum of the dielectric permittivity as a function of

*Corresponding author. Email: claire.laulhe@synchrotron-soleil.fr

temperature, in strong contrast to the sharp and frequency-independent anomalies observed in classic ferroelectrics. With decreasing temperature, most relaxors do not undergo structural phase transition but develop a nanoscale structure that consists in polar atomic displacements with short-range correlations (the so-called polar nanoregions). The directions of displacements are different in distinct polar nanoregions, which leads to a canceled macroscopic polarization.

Chemical substitution was shown to be essential to obtain the relaxor properties, for it introduces spatial fluctuations of bonds and charges [3]. The charge fluctuations, which occur in the case of a heterovalent substitution (e.g. Mg^{2+}/Nb^{5+} in the canonical relaxor $PbMg_{1/3}Nb_{2/3}O_3$), were long considered as the main driving force at the origin of the formation of polar nanoregions [4]. Nevertheless, the relaxor behavior is also observed in several lead-free $BaTiO_3$-based solid solutions with a homovalent substitution, as exemplified by $BaTi_{1-x}Zr_xO_3$ ($0.25 \leq x \leq 0.50$) [5]. Such systems are of fundamental interest, as they offer the opportunity to isolate and study the role of lattice deformations in the appearance of the relaxor behavior.

Accurate descriptions of the atomic structure are crucial for understanding the physical properties of relaxors ferroelectrics. In the perovskite structure of $BaTi_{1-x}Zr_xO_3$, the local dipole moments in the polar nanoregions are related to cation shifts inside their negatively-charged cubo-octahedral or octahedral cages. Besides, distortions of the oxygen atoms' network are expected due to the large difference in the size of the substituted Zr^{4+} and Ti^{4+} cations ($r_{Ti^{4+}} = 0.605$ Å, $r_{Zr^{4+}} = 0.72$ Å) [6]. In ferroelectric compounds, such distortions affect the amplitude and/or orientation of the local dipole moments. In the particular case of $BaTi_{1-x}Zr_xO_3$ relaxors, it has been proposed that the finite correlation length of the local dipole moment orientations is related to chemically-induced random local strains [7–9].

The analysis of the Bragg peaks in $BaTi_{1-x}Zr_xO_3$ relaxors reveals a cubic crystallographic structure [10], in which the Ti and Zr atoms lie at the center of identical, regular octahedra. Due to the assumption of periodicity underlying such an analysis, the cation displacements and structural distortions expected in $BaTi_{1-x}Zr_xO_3$ relaxors are averaged to zero. On the other hand, local structural probes have been proven to overcome such a limitation in the study of relaxor ferroelectrics [11–23]. In this article, we review our investigations of the local structure of $BaTi_{1-x}Zr_xO_3$ relaxors, which were conducted by means of neutron total scattering, EXAFS at the Zr *K*-edge, and supercell *ab-initio* calculations [24–26]. A previously unpublished interpretation of the EXAFS data at the Zr *K*-edge is added, which allows us to properly establish the consistency between those and our more recent *ab-initio* calculations. Our aim is to provide the reader with an accurate and comprehensive description of the structural mechanisms which relate chemical substitution and disordered polar displacements in the $BaTi_{1-x}Zr_xO_3$ system.

In the following, we first consider in Section 2 the pair distribution functions obtained from neutron total scattering, which offer an overall description of the TiO_6 and ZrO_6 octahedra. We show that the local dipole moments in $BaTi_{1-x}Zr_xO_3$ relaxors are mainly due to the Ti atom displacements, and give evidence for a large size difference between the Ti–O_6 and Zr–O_6 oxygen cages. In Section 3, we consider how the Ti–O_6 and Zr–O_6 cages accommodate their size mismatch to form the perovskite structure. Based on previously unpublished fits of the EXAFS data at the Zr *K*-edge and supercell *ab-initio* calculations, we show that the octahedral cages are distorted according to the local Ti/Zr repartition. As shown in Section 4, these distortions influence the polar Ti displacements, which then become constrained in their orientation according to the local Zr/Ti distribution. Our results are finally summarized and discussed in Section 5.

2. Description of the ZrO_6 and TiO_6 octahedral units

In order to give an overall view on the local structure in $BaTi_{1-x}Zr_xO_3$ relaxors, we first consider their pair distribution functions (PDFs). A PDF is obtained as the Fourier transform (FT) of the normalized X-ray or neutron total scattered intensity. It consists in a histogram of all the interatomic distances present in a sample, each pair of atoms giving rise to a peak weighted by the product of their scattering powers [27]. In the case of $BaTi_{1-x}Zr_xO_3$, neutron scattering is particularly suited to study the differences between local structures around Ti- and Zr-atoms; indeed, the opposite signs of Ti and Zr neutron coherent scattering lengths ($\overline{b_{Ti}} = -3.30$ fm and $\overline{b_{Zr}} = 7.16$ fm) result in opposite sign contributions of the Ti–O/Ti–Ba and Zr–O/Zr–Ba pairs to the PDFs.

Figure 1 represents the PDFs of $BaTiO_3$, $BaTi_{0.65}Zr_{0.35}O_3$ (vertical shift +4), and $BaZrO_3$ (vertical shift +8) as determined from neutron total scattering measurements performed on the D4 diffractometer at the Institute Laue-Langevin (ILL). Details about sample preparation and data treatment can be found in [28] and [25], respectively. The weighted sum of the PDFs of $BaTiO_3$ (65%) and $BaZrO_3$ (35%), represented as a line, is superimposed to the PDF of $BaTi_{0.65}Zr_{0.35}O_3$. A remarkable agreement is found in the r-range [1.65–3.25 Å] that corresponds to the Ti–O, Zr–O, and O–O interatomic distances inside TiO_6 and/or ZrO_6 octahedra, and the Ba–O and O–O interatomic distances inside the BaO_{12} cubo-octahedra. This observation implies that the distributions of distances between the closest neighbors remain unchanged in $BaTi_{1-x}Zr_xO_3$ relaxors with respect to the end-members $BaTiO_3$ and $BaZrO_3$. On the contrary, the weighted sum of the PDFs of $BaTiO_3$ and $BaZrO_3$ poorly reproduces the PDF of $BaTi_{0.65}Zr_{0.35}O_3$ beyond 3.25 Å, showing the influence of the chemical substitution on the longer pair arrangements. Similar observations could be made for the $BaTi_{0.68}Zr_{0.32}O_3$ and $BaTi_{0.75}Zr_{0.25}O_3$ relaxors as well [25].

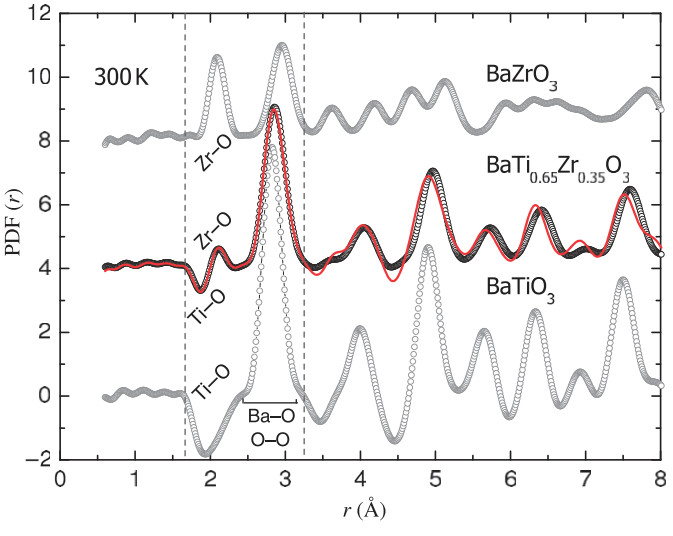

Figure 1. Experimental PDFs of $BaTiO_3$, $BaTi_{0.65}Zr_{0.35}O_3$ (vertical shift +4), and $BaZrO_3$ (vertical shift +8) at 300 K (circles). For $BaTi_{0.65}Zr_{0.35}O_3$, the experimental PDF is compared with the weighted sum of the experimental PDFs of $BaTiO_3$ (65%) and $BaZrO_3$ (35%). A remarkable agreement is found in the r-range [1.65–3.25 Å] delimited by the two vertical dashed lines.

The Ti–O (resp. Zr–O) and O–O distance distributions are related to the structure of the TiO_6 (resp. ZrO_6) octahedra. Even if the information on interatomic distances does not allow a complete description of the structure in three dimensions, the similarity of the Ti–O and Zr–O distance distributions $BaTi_{1-x}Zr_xO_3$ and in $BaTiO_3$/$BaZrO_3$ suggests that the TiO_6 and ZrO_6 octahedra are similar in $BaTi_{1-x}Zr_xO_3$ relaxors and in the end-member compounds. As a result, it is possible to discuss both the Ti/Zr displacements and the deformation of the O_6 cages in $BaTi_{1-x}Zr_xO_3$ relaxors from the known structures of $BaTiO_3$ and $BaZrO_3$.

TiO_6 octahedra: The classic ferroelectric $BaTiO_3$ undergoes three structural phase transitions as the temperature decreases: cubic to tetragonal at 393 K, tetragonal to orthorhombic at 278 K, and orthorhombic to rhombohedral at 183 K. It was shown that despite these changes in macroscopic symmetry, at 300 K the TiO_6 octahedra present a similar structure as in the low-temperature rhombohedral phase [29]. In the structure reported for $BaTiO_3$ at 15 K, the Ti atoms are shifted by 0.18 Å in the $[111]_p$ direction of the pseudo-cubic perovskite unit cell, i.e. toward a face of their octahedron [30]. The average Ti–O distance is found equal to 2.03 Å. In view of transposing this structure to the case of $BaTi_{1-x}Zr_xO_3$ relaxors, it is nevertheless important to note that the PDF gives a Ti–O distance distribution that is averaged on all the Ti sites. In relaxor compounds, the existence of disordered Ti displacements is probable and in this case, the aforementioned Ti displacement characteristics apply to a *mean* Ti displacement vector. Moreover, the limited *r*-resolution of our PDFs and the superposition of the Ti–O and Zr–O pair contributions prevent from clearly distinguishing (average) Ti displacements in the [111] direction or in other directions. In any case, the very broad Ti–O distance distribution [1.65–2.45 Å] is a signature of large Ti polar displacements.

ZrO_6 octahedra: $BaZrO_3$ crystallizes in the ideal, cubic $Pm\bar{3}m$ perovskite structure, with a cell parameter equal to 4.194 Å [31,32]. In this compound, the local structure is considered to be identical to the cubic crystallographic structure [33]. The Zr atoms thus lie at the center of regular oxygen octahedra, the mean Zr–O distance being equal to 2.10 Å.

By transposing this description of the TiO_6 and ZrO_6 octahedra to the case of $BaTi_{1-x}Zr_xO_3$ relaxors, we can conclude that the Ti atoms, unlike the Zr atoms, are largely displaced in their octahedra and hence play a significant role in the local polarization. Moreover, the ZrO_6 and TiO_6 octahedra, which coexist in $BaTi_{1-x}Zr_xO_3$ relaxors, exhibit very different sizes (mean Ti–O distance: 2.03 Å, mean Zr–O distance: 2.10 Å).

3. Accommodation of TiO_6 and ZrO_6 size mismatch in $BaTi_{1-x}Zr_xO_3$ relaxors

3.1. *EXAFS study at the Zr K-edge*

Despite their large size difference, the Ti–O_6 and Zr–O_6 oxygen cages link together to form the perovskite structure. This implies that they undergo small and fluctuating distortions with respect to the average structures described above. A first step toward the description of these distortions is to determine the Ti–Ti, Ti–Zr, and Zr–Zr distances that characterize the link between octahedra in $BaTi_{1-x}Zr_xO_3$ relaxors. In PDFs, however, all those pairs contribute in the same *r*-range [3.70–4.40 Å], together with the Ba–Ba and O–O pairs (Figure 1). To overcome this difficulty, we considered the partial distribution functions as given by Extended X-ray Absorption Fine Structure (EXAFS). In the case of $BaTi_{1-x}Zr_xO_3$, the Zr–Zr and Zr–Ti distances are accessible from the analysis of EXAFS at the Zr *K*-edge. Unfortunately, the Ti–Ti distance cannot be obtained from EXAFS data at the Ti *K*-edge, since the presence of the Ba L_{III} edge prevents measuring the EXAFS

oscillations at the Ti *K*-edge in a sufficiently large energy range. In the following, we will consider solely X-ray absorption experiments at the Zr *K*-edge which were carried out on the FAME-BM30B beamline at the European Synchrotron Radiation Facility (ESRF) on several $BaTi_{1-x}Zr_xO_3$ relaxors ($x = 0.25$, 0.30, and 0.35), and on $BaZrO_3$ for reference purposes. The EXAFS data were collected at room temperature for all samples, as well as at 10 K for $BaZrO_3$ and at 10 K, 90 K, and 150 K for $BaTi_{0.65}Zr_{0.35}O_3$. Details on sample preparation and extraction of the experimental EXAFS signals can be found in [28] and [24], respectively.

An EXAFS experiment consists in measuring the energy dependence of the X-ray absorption coefficient near an absorption edge of a given atom in the sample. The scattering of the photoelectron by the neighbors of the central absorbing atom introduces oscillations of the absorption coefficient after the energy edge. The EXAFS signal $\chi(k)$ is defined as the oscillatory part of the absorption coefficient, k being the photoelectron wavenumber. It depends on the local structure around the absorbing atom and is expressed as a sum of contributions from different paths, each path i corresponding to a given scattering process of the photoelectron [34]:

$$\chi(k) = -S_0^2 \sum_i \frac{N_i A_i(k)}{k R_i^2} e^{-2k^2\sigma_i^2} e^{-2R_i/\lambda(k)} \sin(2kR_i + 2\delta_c(k) + \phi_i(k)),$$

where N_i is the degeneracy of path i, R_i its half-length and $A_i(k)$ its effective scattering amplitude. The Debye–Waller (DW) factor σ_i^2 is the standard deviation of the R_i distance distribution, assumed to be Gaussian. It takes into account both the thermal disorder and a possible small structural disorder. $\delta_c(k)$ and $\phi_i(k)$ are phase shifts associated with the electron propagating into and out the potentials of the absorbing site and scattering sites, respectively. The other parameters are the photoelectron mean-free path $\lambda(k)$ and an overall amplitude factor S_0^2, close to 1, which accounts for many-electron effects in the excited central atom. Values of the structural parameters N_i, R_i, and σ_i^2 can be obtained by fitting $\chi(k)$ to the experimental EXAFS signal.

The amplitudes and phases of all possible scattering paths were calculated by using the FEFF8.00 code [35], for an atomic cluster of 145 atoms representative of the $Pm\bar{3}m$ perovskite structure of $BaZrO_3$. In order to take into account the Ti atoms present in $BaTi_{1-x}ZrO_3$, paths were also determined for a hypothetical cluster of $BaTiO_3$ in the $Pm\bar{3}m$ perovskite structure with a single Zr impurity as the absorbing atom. In our fitting procedure we kept only the paths with a relative amplitude higher than 2.5%, since they are the only ones that significantly contribute to the calculated $\chi(k)$. They are represented in Figure 2.

The FTs of selected k^2-weighted experimental EXAFS signals calculated in the R-range [0–5 Å], as described in [24], are given in Figure 3.[1] The first contribution to the FTs, at R-values lower than 2.5 Å, includes only a back-scattering process on one of the six first oxygen (O) neighbors of the central Zr atom (path 1 in Figure 2). The second contribution found in the R-range [2.5–4.5 Å] results both from back-scattering processes on the second (Ba), third (Zr or Ti), or fourth oxygen (O2) neighbors of the Zr atom (paths 1, 2, 3, and 10 in Figure 2), and from several multiple scattering processes (paths 4–9 in Figure 2).

One can see in Figure 3 that the first peak of the FTs is nearly identical at 300 K in all relaxor samples and in $BaZrO_3$, which suggests very close first neighbor environments of the Zr atoms whatever the Zr substitution rate. Fits to the experimental EXAFS signals in the R-range [1.14–2.33 Å], which were published in [24], showed that indeed

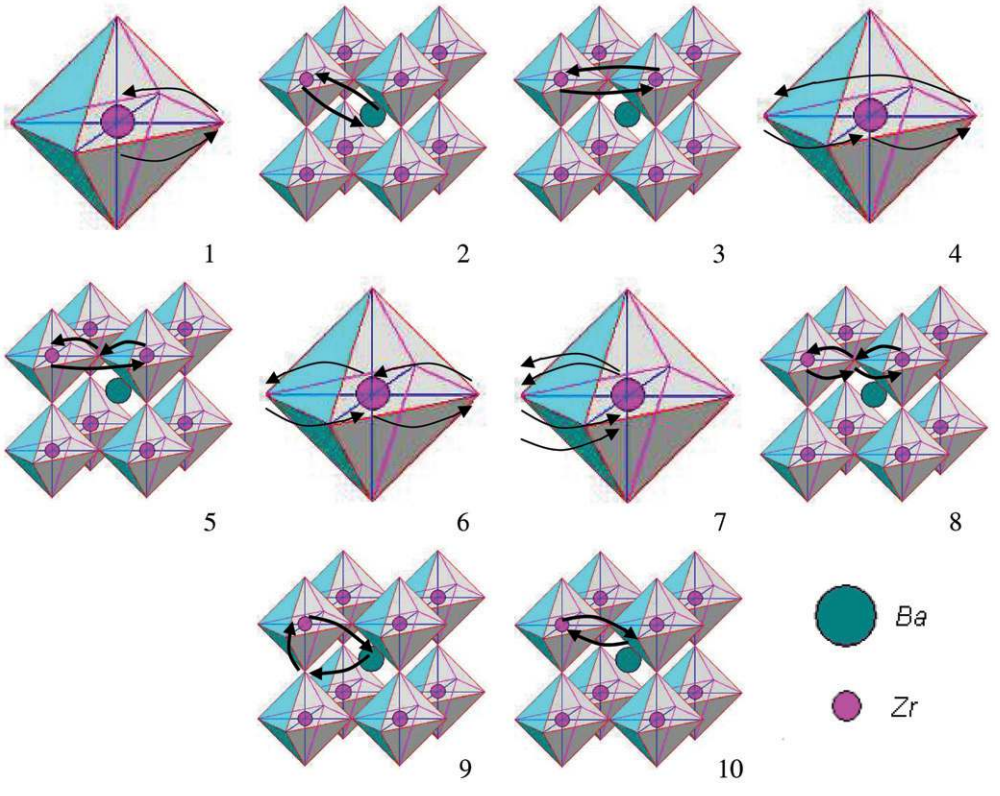

Figure 2. Representation of the photoelectron scattering paths that contribute to the first and second peaks of the FT modulii of the EXAFS signal, determined for $BaZrO_3$ by using the FEFF8.00 code. The oxygen atoms, which are not represented, lie at the corners of the octahedra. When considering the EXAFS signal of $BaTi_{1-x}Zr_xO_3$ relaxors, one has to take into account 3′, 5′, and 8′ paths for which the backscattering Zr atoms are replaced with Ti ones.

the mean Zr–O distance is equal in all the $BaTi_{1-x}Zr_xO_3$ relaxors studied ($x = 0.25$, 0.30, and 0.35) and in $BaZrO_3$. This result is fully consistent with the conclusions obtained from the PDF analysis. On the other hand, the DW factors fitted in the same study for the Zr–O distances were found to be systematically higher in $BaTi_{1-x}Zr_xO_3$ relaxors than in $BaZrO_3$. This observation is interpreted as the signature of a small static distribution of the Zr–O distances in relaxor samples which does not exist in $BaZrO_3$, with a full width at half maximum in the range [0.05–0.06 Å] depending on the Zr substitution rate.[2] This static distribution of the Zr–O distances could be due to either deformations of the Zr–O_6 oxygen cages, or a small displacement of the Zr atoms inside their oxygen cages. In the latter case, the displacement amplitude would be below 0.05 Å [36].

For R-values larger than 2.5 Å, the FTs of $BaZrO_3$ and $BaTi_{1-x}Zr_xO_3$ relaxors differ significantly. This can be explained by the presence of Ti third neighbors in the relaxor samples, as well as distortions caused by the Ti/Zr size difference. In order to characterize the local structure of $BaTi_{1-x}Zr_xO_3$ relaxors beyond the ZrO_6 octahedron's scale, we fitted calculated FTs to the experimental ones in the R-range [1.14–4.52 Å] (24.16 independent points), by using the FEFFIT program [37]. The parameter ΔE_0, which takes into account

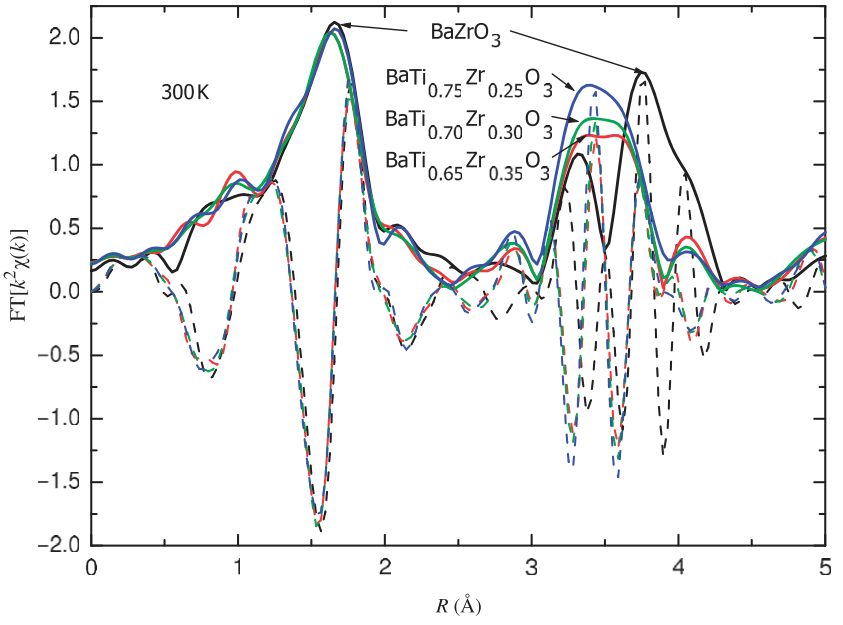

Figure 3. FTs of the k^2-weighted Zr *K*-edge EXAFS signals of $BaZrO_3$, $BaTi_{0.75}Zr_{0.25}O_3$, $BaTi_{0.70}Zr_{0.30}O_3$, and $BaTi_{0.65}Zr_{0.35}O_3$ at 300 K. The imaginary part and the modulus of the FTs are plotted with dashed and solid lines, respectively.

the small difference between the experimental edge energy E_0 and its value calculated by FEFF8.00, was fixed to the value found in [24], as well as S_0^2. We constructed a structural model based on the scattering paths represented in Figure 2. The electronic parameters $A_i(k)$, $\phi_i(k)$, $\delta_c(k)$, and $\lambda(k)$ were calculated with the FEFF8.00 code. The path degeneracies were assumed to be the same as in an ideal $Pm\bar{3}m$ perovskite structure. A parameter N_{Zr} was introduced, which represents the average number of Zr neighbors around the Zr central atom. Its value was fixed to $6x$, the value expected in the case of a random Zr/Ti substitution. All the *mean* interatomic distances (d_{Zr-O}, d_{Zr-Ba}, d_{Zr-Ti}, d_{Zr-Zr}, and d_{Zr-O2}) were supposed to be independent. However, note that this model can only probe expansion/compression deformations, i.e. atoms in the Zr–O–Ti and Zr–O–Zr chains are assumed to be aligned. In the case of angularly deformed Zr–O–Ti and Zr–O–Zr chains indeed, the amplitude parameters of the multiple scattering paths 5, 5′, 8, and 8′ would have to be modified [38]. Finally, we took into account the relations that exist between the DW factors of the different paths [24] in order to minimize the number of fitted parameters. Relations between local structure parameters and path parameters are summarized in Table 1. The d_{Zr-O} and σ_O^2 parameters being fixed to the values obtained from a separate fit in the *R*-range [1.14–2.33 Å] [24], eight parameters were refined: d_{Zr-Ba}, σ_{Ba}^2, d_{Zr-Ti}, σ_{Ti}^2, d_{Zr-Zr}, σ_{Zr}^2, d_{Zr-O2}, and σ_{O2}^2. The calculated FTs obtained for this structural model are in excellent agreement with the experimental ones at all temperatures (Figure 4). The refined value of each parameter is presented in Table 2.

A value of 4.153 ± 0.005 Å is found for the d_{Zr-Zr} distance in $BaTi_{0.65}Zr_{0.35}O_3$. Reminding our hypothesis of linear Zr–O–Zr chains, the two Zr–O distances can be estimated at $d_{Zr-Zr}/2 = 2.08$ Å. The latter value is slightly shorter than the mean Zr–O distance ($d_{Zr-O} = 2.10$ Å), but belongs to the interval [2.04–2.16 Å] of the aforementioned static distribution of the Zr–O distances. In the framework of the present model, one can

Table 1. Relation between paths parameters and structural parameters in the model used to analyze the EXAFS data of $BaTi_{1-x}Zr_xO_3$ relaxors.

Index	Scattering process	N_i	R_i	σ_i^2
1	$Zr_c \rightarrow O \rightarrow Zr_c$	6	d_{Zr-O}	σ_O^2
2	$Zr_c \rightarrow Ba \rightarrow Zr_c$	8	d_{Zr-Ba}	σ_{Ba}^2
3	$Zr_c \rightarrow Zr \rightarrow Zr_c$	N_{Zr}	d_{Zr-Zr}	σ_{Zr}^2
3′	$Zr_c \rightarrow Ti \rightarrow Zr_c$	(6-N_{Zr})	d_{Zr-Ti}	σ_{Ti}^2
4	$Zr_c \rightarrow O' \rightarrow O \rightarrow Zr_c$	6	$2d_{Zr-O}$	σ_O^2
5	$Zr_c \rightarrow Zr \rightarrow O \rightarrow Zr_c$	2 N_{Zr}	d_{Zr-Zr}	σ_{Zr}^2
5′	$Zr_c \rightarrow Ti \rightarrow O \rightarrow Zr_c$	2 (6-N_{Zr})	d_{Zr-Ti}	σ_{Ti}^2
6	$Zr_c \rightarrow O' \rightarrow Zr_c \rightarrow O \rightarrow Zr_c$	6	$2d_{Zr-O}$	σ_O^2
7	$Zr_c \rightarrow O \rightarrow Zr_c \rightarrow O \rightarrow Zr_c$	6	$2d_{Zr-O}$	$2\sigma_O^2$
8	$Zr_c \rightarrow O \rightarrow Zr \rightarrow O \rightarrow Zr_c$	N_{Zr}	d_{Zr-Zr}	σ_{Zr}^2
8′	$Zr_c \rightarrow O \rightarrow Ti \rightarrow O \rightarrow Zr_c$	(6-N_{Zr})	d_{Zr-Ti}	σ_{Ti}^2
9	$Zr_c \rightarrow Ba \rightarrow O \rightarrow Zr_c$	48	$\frac{d_{Zr-O}(1+\sqrt{2})+d_{Zr-Ba}}{2}$	σ_O^2
10	$Zr_c \rightarrow O2 \rightarrow Zr_c$	24	d_{Zr-O2}	σ_{O2}^2

Note: Zr_c denotes the central absorbing Zr atom.

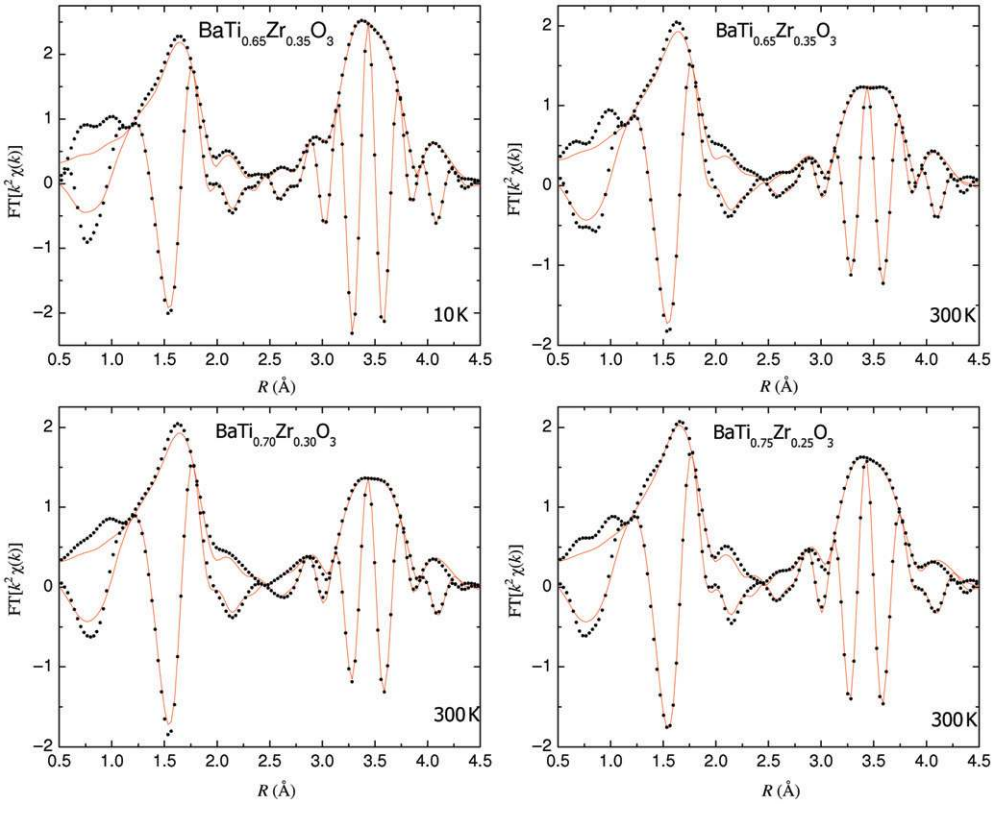

Figure 4. Modulus and imaginary part of the FT of $k^2\chi(k)$ at either 10 K or 300 K, for $BaTi_{1-x}Zr_xO_3$ relaxors. The dots represent measured data and the solid lines their best fit, obtained with the parameters values given in Table 1.

Table 2. Structural parameters deduced from the EXAFS analysis in the R-range [1.14–4.52 Å], for $BaTi_{1-x}Zr_xO_3$ relaxors.

	$x = 0.35$				$x = 0.30$	$x = 0.25$
	10 K	90 K	150 K	300 K	300 K	300 K
d_{Zr-O} (Å)	2.096	2.098	2.096	2.099	2.101	2.104
σ^2_O (Å^2)	0.0035	0.0038	0.0038	0.0048	0.0048	0.0043
d_{Zr-Ba} (Å)	3.565	3.566	3.565	3.568	3.564	3.556
σ^2_{Ba} (Å^2)	0.0037	0.0042	0.0049	0.0072	0.0069	0.0059
d_{Zr-Zr} (Å)	4.145	4.149	4.148	4.153	4.153	4.159
σ^2_{Zr} (Å^2)	0.0021	0.0023	0.0025	0.0040	0.0039	0.0041
d_{Zr-Ti} (Å)	4.088	4.092	4.089	4.093	4.088	4.081
σ^2_{Ti} (Å^2)	0.005	0.005	0.006	0.008	0.008	0.008
d_{Zr-O2} (Å)	4.58	4.58	4.58	4.59	4.58	4.58
σ^2_{O2} (Å^2)	0.009	0.009	0.010	0.013	0.014	0.012
RF (%)	0.35	0.67	0.56	0.83	0.74	0.56

Notes: The values found in [24] for d_{Zr-O} and σ^2_O are recalled but were fixed during the fitting procedure to the values found in [24]. The uncertainties are of the order of ±0.003 Å, ±0.0002 Å^2, ±0.007 Å, ±0.0004 Å^2, ±0.005 Å, ±0.001 Å^2, ±0.01 Å, ±0.002 Å^2 for d_{Zr-Ba}, σ^2_{Ba}, d_{Zr-Ti}, σ^2_{Ti}, d_{Zr-Zr}, σ^2_{Zr}, d_{Zr-O2}, and σ^2_{O2}, respectively. The reliability of fit (RF) given by FEFFIT is reported on the last line.

assume that Zr–O–Zr bondings involve two short Zr–O distances from the 0.06 Å wide static distribution, and hence that the Zr–O–Ti bondings involve the longest Zr–O distances. The EXAFS data are thus compatible with a model of the local structure where the Zr–O_6 octahedral cages are compressed in the direction of Zr neighbors, and expanded in the direction of Ti neighbors (Figure 5a). The mean Zr–Ti distance d_{Zr-Ti} is refined to 4.093 Å in $BaTi_{0.65}Zr_{0.35}O_3$. In the hypothesis that the longest [2.10–2.16 Å] Zr–O distances are involved in the Zr–O–Ti bonding, the expected values of Ti–O distances fall in the interval [1.93–1.99 Å]. These values are lower than the mean Ti–O distance measured from the PDFs (2.03 Å), which can be interpreted in two possible ways: (1) the Ti–O_6 oxygen cages are compressed in the direction of Zr neighbors, and/or (2) the Ti atoms preferably shift toward their Zr neighbors. Similar conclusions can be obtained for all $BaTi_{1-x}Zr_xO_3$ relaxors studied. Moreover, our results show that the local structure hardly changes as the temperature decreases down to 10 K.

A d_{Zr-Zr} distance shorter than twice the d_{Zr-O} can also be obtained through angular deformations of the Zr–O–Zr chains. It was shown that a structural model based on such deformations allows an excellent agreement between calculated and experimental FTs of the EXAFS signal of $BaTi_{1-x}Zr_xO_3$ relaxors [24]. The refined values of the buckling angles of the Zr–O-Zr and Zr–O–Ti chains then differ significantly (∼19° and less than 10°, respectively).[3] In this model, the ZrO_6 octahedra thus undergo angular distortions, the amplitude of which directly depends on the local Ti/Zr repartition (Figure 5b).

In conclusion, EXAFS experiments at the Zr K-edge do not allow determining the nature of the distortions caused by the assemblage of small Ti–O_6 and large Zr–O_6 oxygen cages in the perovskite structure of $BaTi_{1-x}Zr_xO_3$ relaxors. However, they provide evidence that the Zr–O_6 oxygen cages are distorted depending on the local distribution of

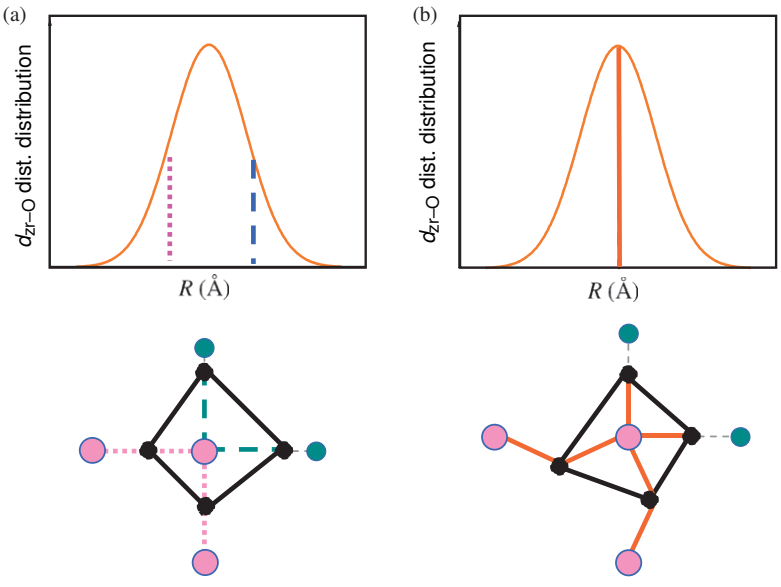

Figure 5. Planar schematic view of ZrO_6 octahedra distortions in $BaTi_{1-x}Zr_xO_3$ relaxors. The oxygen cages are represented in black, while the Ti and Zr atoms appear in light magenta and dark green, respectively. In the present model (a), the length of a Zr–O bond depends on the chemical nature of the facing neighbor. As a result, the ZrO_6 octahedra are compressed/elongated according to the local Ti/Zr distribution. In the model presented in [24] (b), the Zr–O distances fluctuate, but there is no relation between their length and the chemical environment. In this case, however, the ZrO_6 octahedra undergo angular distortions, the amplitude of which depends on the local Ti/Zr distribution. Note that both the (a) and (b) models yield a very good agreement between the calculated and experimental FTs of the EXAFS signals.

Ti and Zr atoms. Similar information remains unknown for the Ti–O_6 oxygen cages, due to the inaccessibility to proper EXAFS data at the Ti *K*-edge.

3.2. *Supercell* ab-initio *calculations*

To gain further insight into the Ti–O_6 and Zr–O_6 oxygen cage distortions and their dependence on the local Ti/Zr distribution, we performed supercell *ab-initio* calculations on the $BaTi_{0.74}Zr_{0.26}O_3$ relaxor [26]. Atomic positions were optimized in three 135-atom supercells representing three different averaged chemical short range arrangements, starting from the cubic $Pm\bar{3}m$ perovskite structure. We then studied the dependence of the local structure on the Ti/Zr distribution by means of a statistical analysis of the relaxed supercells.

The angular distortions of octahedra are found smaller than 1°, which precludes the structural model with different buckling angles of the Zr–O–Zr and Zr–O–Ti chains (Figure 5b). On the other hand, distortions that involve elongations and/or compressions of the O_6 cages are clearly evidenced. Figure 6 shows the calculated G–O distance distributions inside the TiO_6 and ZrO_6 octahedra, G being the center of mass of the six oxygen atoms that form an octahedron. The G–O distances in G–O–Ti and G–O–Zr chains are separated and represented in dark green and light magenta, respectively. It is found that the shortest G–O distances are observed when the neighboring octahedral site is

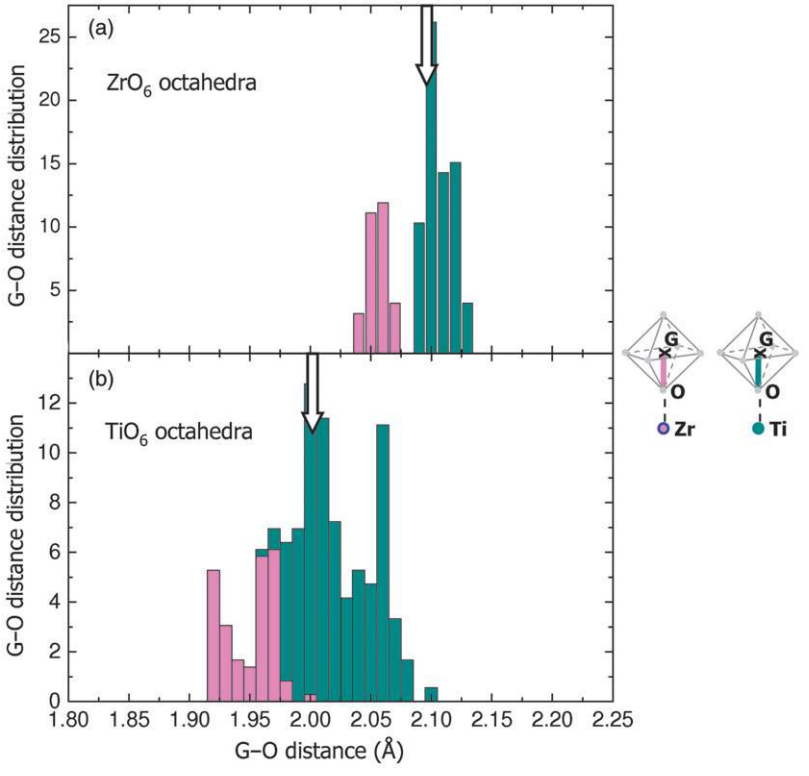

Figure 6. Distribution of the distance between the center of mass of oxygens (denoted G) and the oxygens calculated from the relaxed supercells of $BaTi_{0.74}Zr_{0.26}O_3$: (a) for the Zr–O_6 octahedra and (b) for the Ti–O_6 octahedra. The G–O segments that are directed toward Zr and Ti neighbors are represented in light magenta and dark green, respectively. The arrows mark the mean G–O distances calculated for the Zr–O_6 and Ti–O_6 octahedra.

occupied by a Zr atom, while the longest ones occur when the neighboring octahedral site is occupied by a Ti atom. Hence, ZrO_6 and TiO_6 octahedra are compressed in the direction of Zr neighbors, and expanded in the direction of Ti neighbors. Concerning ZrO_6 octahedra, this conclusion perfectly corresponds to the first structural model discussed in Section 3.1 (Figure 5a).

4. Strain effects on the local dipole moments

In ferroelectric materials, a close relation exists between atomic polar displacements and strain [39]. The chemically-induced compression/elongation distortions of the Ti–O_6 oxygen cages are thus expected to lead to disordered Ti polar displacements in $BaTi_{1-x}Zr_xO_3$ relaxors, which would be at least partly determined by the local Zr/Ti distribution. In order to investigate this point, the Ti displacement vectors away from the center of mass of their surrounding oxygen cages were calculated from the relaxed supercells of $BaTi_{0.74}Zr_{0.26}O_3$. They are represented in Figure 7, the x-, y-, and z-axes being parallel to the Cartesian axes of the supercell (i.e., parallel to the octahedra's axes before structural relaxation). One can first observe that the Ti atoms with six Ti neighbors are displaced in one of the eight ⟨111⟩ directions, as it is the case in $BaTiO_3$ (Figure 7a). When

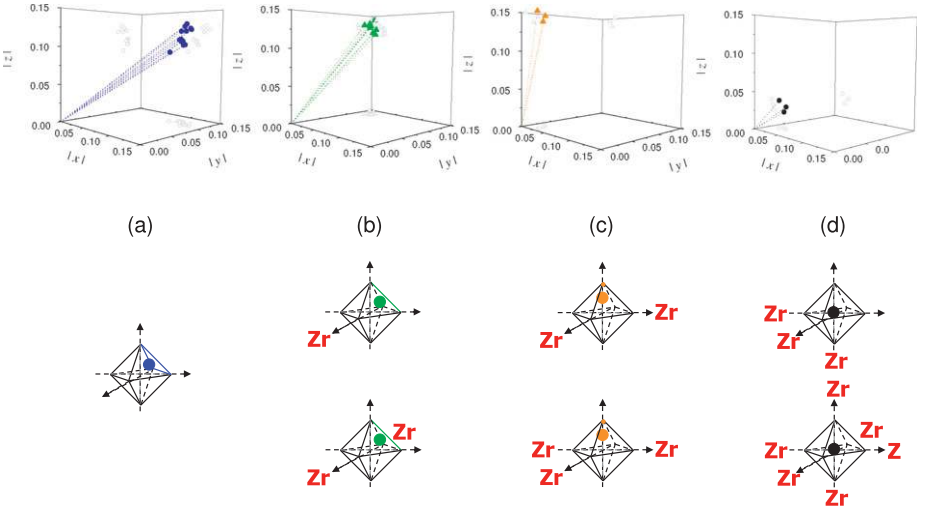

Figure 7. Ti displacement vectors calculated in the relaxed supercells of the $BaTi_{1-x}Zr_xO_3$ relaxor, represented with the absolute values of their coordinates (closed symbols). The displacement vector projections in the (x,y), (y,z), and (x,z) planes are also given to ease visualization (open symbols). Four types of chemical environments are considered, as illustrated in the bottom part of the figure: (a) the TiO_6 octahedron is surrounded only by Ti neighbors, (b) one or two Zr neighbors are present on the x-axis of the TiO_6 octahedron, (c) one or two Zr neighbors are present on each of the x- and y-axes of the TiO_6 octahedron, and (d) one or two Zr neighbors are present on each of the x-, y-, and z-axes of the TiO_6 octahedron. For the sake of clarity, only the Zr neighbors are represented for a given TiO_6 unit.

there are one or two Zr neighbors lying on the x-axis (Figure 7b), the polar Ti displacements are found to be systematically oriented in the four [011], [0$\bar{1}$1], [01$\bar{1}$], and [0$\bar{1}\bar{1}$] directions, i.e. there is no displacement component on the Zr neighbors' axis. Consistently, the presence of Zr neighbors on both the x- and y-axes leads to Ti displacements in the two [001] and [00$\bar{1}$] directions (Figure 7c). Finally, the Ti atoms with Zr neighbors on the three x-, y-, and z-axes are found to be almost not displaced (Figure 7d). Considering the Zr-induced local compression of the oxygen cages (Section 3.2), one can conclude that the local Ti/Zr distribution determines the Ti displacement symmetries through strain effects.

5. Conclusion

The local structure in $BaTi_{1-x}Zr_xO_3$ relaxors was investigated by using a combination of experimental and theoretical methods, namely neutron total scattering, X-ray absorption spectroscopy, and supercell *ab-initio* calculations. As the main characteristic of the local structure in this material, the interatomic distances between first neighbors tend to keep the same length as in the end-member compounds. In particular, the TiO_6/ZrO_6 octahedra are found to exhibit similar structures in $BaTi_{1-x}Zr_xO_3$ relaxors and in $BaTiO_3/BaZrO_3$. The very wide distribution of the Ti–O distances [1.65–2.45 Å] is the signature of large Ti polar displacements. On the contrary, the distribution width of the Zr–O distances in ZrO_6 octahedra is quite narrow (0.05 to 0.06 Å), and indicates very small Zr displacements if any. The Ti atoms thus play a major role in the local polarization of $BaTi_{1-x}Zr_xO_3$

relaxors, unlike the Zr atoms. By considering the mean Ti–O and Zr–O distances (2.03 and 2.10 Å, respectively), we establish that the Ti–O_6 and Zr–O_6 oxygen cages exhibit very different sizes. When linking to construct the perovskite structure of $BaTi_{1-x}Zr_xO_3$ relaxors, each of the small Ti–O_6 and large Zr–O_6 oxygen cages undergo distortions which depend on the nature of the neighboring octahedra (TiO_6 or ZrO_6). It is found that the Ti–O_6 and Zr–O_6 oxygen cages are slightly compressed (expanded) in the direction of Zr (Ti) neighbors, respectively. The oxygen atoms' network is thus subjected to chemically-induced strains, which were found to be coupled with the Ti local dipole moments. While the preferred orientation for a Ti displacement is the ⟨111⟩ in the absence of Zr neighbors, a displacement component is canceled as soon as a neighboring Zr atom lies on the corresponding octahedron's axis. As a result, the Ti atoms exhibit displacements in the ⟨111⟩, ⟨011⟩, and ⟨001⟩ directions, or no displacement at all, depending on the local Ti/Zr repartition. Such a variety of the Ti polar displacement orientations in $BaTi_{1-x}Zr_xO_3$ relaxors impedes a perfect alignment of the local dipole moments as it exists in the classic ferroelectric $BaTiO_3$. Nevertheless, the chemical environment only determines the symmetry of a Ti displacement, and several shifting directions remain available unless Zr atoms lie on each of the three octahedron's axes. This degree of freedom allows partial correlations of the polar displacements, and thus the formation of polar nanoregions. Based on an electronic diffraction experiment, Liu et al. [40] reported the observation of *temperature-independent* diffuse scattering lines in the $BaTi_{0.70}Zr_{0.30}O_3$ relaxor, which are similar to those observed in the paraelectric phase of the classic ferroelectric $BaTiO_3$ [41,42]. These observations suggest that the polar nanoregions in $BaTi_{1-x}Zr_xO_3$ relaxors consist in 1D-chains with correlated Ti displacements. As the temperature decreases, Ti displacements on distinct chains remain independent. In strong contrast, Ti displacements correlate from chain to chain in $BaTiO_3$, leading to the disappearance of diffuse scattering lines at 183 K, simultaneously with the transition to the rhombohedral structure in which all the Ti displacements are perfectly aligned. As the next step toward understanding the origin of the relaxor behavior in $BaTi_{1-x}Zr_xO_3$ and other homovalent-substituted $BaTiO_3$-based relaxors, one has to investigate more deeply the ferroelectric to relaxor crossover [5], as well as the formation and growth of the polar nanoregions. For that purpose, a theoretical model should be proposed which takes into account the local constraints on the Ti polar displacements, as well as the elastic and electrostatic interactions that occur on the medium- and long-range scales. In this article, we reported a detailed description of the local constraints that affect the Ti local dipole moments in $BaTi_{1-x}Zr_xO_3$ and probably in other $BaTiO_3$-based relaxors with homovalent substitution. We believe that the results reported here constitute an important step toward the development of such models.

Notes

1. Note that due to the k-dependence of the phase shifts $\delta_c(k)$ and $\phi_i(k)$, the maxima of the FT modulii occur at distances which are different from the real ones.
2. Such a small static distribution of the Zr–O distances cannot be evidenced from the PDFs shown in Section 2, due to the overlap of the Ti–O and Zr–O contributions.
3. Local structure determinations by EXAFS can become model-dependent, especially when a large number of structural parameters are involved. In the present case, N_{Zr}, σ^2_{Zr}, σ^2_{Ti}, and the $Zr\widehat{O}Ti$ / $Zr\widehat{O}Zr$ buckling angles determine the amplitude of the FT modulus in the range [3.4–3.9 Å], which impedes the discrimination of angular and linear deformations of the Zr–O–Zr and Zr–O–Ti chains.

References

[1] A.A. Bokov and Z.G. Ye, *Recent progress in relaxor ferroelectrics with perovskite structure*, J. Mater. Sci. 41 (2006), pp. 31–52.

[2] S.E. Park and T.R. Shrout, *Ultrahigh strain and piezoelectric behavior in relaxor based ferroelectric single crystals*, J. Appl. Phys. 82 (1997), p. 1804.

[3] R. Blinc, A. Gregorovic, B. Zalar, R. Pirc, V.V. Laguta, and M.D. Glinchuk, *^{207} Pb NMR study of the relaxor behavior in $PbMg_{1/3}Nb_{2/3}O_3$*, Phys. Rev. B 63 (2000), p. 024104.

[4] V. Westphal, W. Kleemann, and M.D. Glinchuk, *Diffuse phase transitions and random-field-induced domain states of the "relaxor" ferroelectric $PbMg_{1/3}Nb_{2/3}O_3$*, Phys. Rev. Lett. 68 (1992), p. 847.

[5] A. Simon, J. Ravez, and M. Maglione, *The crossover from a ferroelectric to a relaxor state in lead-free solid solutions*, J. Phys. Condens. Matter 16 (2004), pp. 963–970.

[6] R.D. Shannon, *Revised effective ionic radii and systematic studies of interatomic distances in halides and chalcogenides*, Acta Crystallogr. A 32 (1976), pp. 751–767.

[7] M.D. Glinchuk and R. Farhi, *A random field theory based model for ferroelectric relaxors*, J. Phys. Condens. Matter 8 (1996), pp. 6985–6996.

[8] R. Farhi, M.E. Marssi, A. Simon, and J. Ravez, *Relaxor-like and spectroscopic properties of niobium modified barium titanate*, Europ. Phys. J. B 18 (2000), pp. 605–610.

[9] V.V. Shvartsman, W. Kleemann, J. Dec, Z.K. Xu, and S.G. Lu, *Diffuse phase transition in $BaTi_{1-x}Sn_xO_3$ ceramics: An intermediate state between ferroelectric and relaxor behavior*, J. Appl. Phys. 99 (2006), p. 124111.

[10] T.N. Verbitskaia, G.S. Zhdanov, I.N. Venevstev, and S.P. Soloviev, *Electrical and X-ray diffraction studies of the $BaTiO_3$-$BaZrO_3$ system*, Sov. Phys. Crystallogr. 3 (1958), pp. 182–192.

[11] E. Prouzet, E. Husson, N. Mathande, and A. Morell, *A low-temperature extended X-ray absorption study of the local order in simple and complex perovskites: II. PMN ($PbMg_{1/3}Nb_{2/3}O_3$)*, J. Phys. Condens. Matter 5 (1993), pp. 4889–4902.

[12] I.W. Chen, P. Li, and Y. Wang, *Structural origin of relaxor perovskites*, J. Phys. Chem. Solids 57 (1996), pp. 1525–1536.

[13] V.A. Shuvaeva, I. Pirog, Y. Azuma, K. Yagi, K. Sakaue, H. Terauchi, I.P. Raevskii, K. Zhuchkov, and M.Y. Antipin, *The local structure of mixed-ion perovskites*, J. Phys. Condens. Matter 15 (2003), pp. 2413–2421.

[14] A.I. Frenkel, D.M. Pease, J. Giniewicz, E.A. Stern, D.L. Brewe, M. Daniel, and J. Budnick, *Concentration dependent short-range order in the relaxor ferroelectric $(1-x)Pb(Sc, Ta)O_{3-x}PbTiO_3$*, Phys. Rev. B 70 (2004), p. 014106.

[15] V.A. Shuvaeva, D. Zekria, A.M. Glazer, Q. Jiang, S.M. Weber, P. Bhattacharya, and P.A. Thomas, *Local structure of the lead-free relaxor ferroelectric $(K_xNa_{1-x})_{0.5}Bi_{0.5}TiO_3$*, Phys. Rev. B 71 (2005), p. 174114.

[16] H.D. Rosenfeld and T. Egami, *Short and intermediate range structural and chemical order in the relaxor ferroelectric lead magnesium niobate*, Ferroelectrics 164 (1995), pp. 133–141.

[17] S. Teslic, T. Egami, and D. Viehland, *Local atomic structure of PZT and PLZT studied by pulsed neutron scattering*, J. Phys. Chem. Solids 57 (1996), pp. 1537–1543.

[18] T. Egami, W. Dmowski, M. Akbas, and P.K. Davies, *Local structure and polarization in Pb containing ferroelectric oxides*, AIP Conf. Proc. 436 (1998), pp. 1–10.

[19] W. Dmowski, M.K. Akbas, P.K. Davies, and T. Egami, *Local structure of $Pb(Sc_{1/2}, Ta_{1/2})O_3$ and related compounds*, J. Phys. Chem. Solids 61 (2000), pp. 229–237.

[20] P. Juhas, I. Grinberg, A.M. Rappe, W. Dmowski, T. Egami, and P.K. Davies, *Correlations between the local structure and dielectric properties of $Pb(Sc_{2/3}W_{1/3})O_3$-$Pb(Ti/Zr)O_3$ relaxors*, Phys. Rev. B 69 (2004), p. 214101.

[21] I.K. Jeong, T.W. Darling, J.K. Lee, T. Proffen, R.H. Heffner, J.S. Park, K.S. Hong, W. Dmowski, and T. Egami, *Direct observation of the formation of polar nanoregions in $Pb(Mg_{1/3}Nb_{2/3})O_3$ using neutron pair distribution function analysis*, Phys. Rev. Lett. 94 (2005), p. 147602.

[22] I.K. Jeong, J.K. Lee, and R.H. Heffner, *Local structural view on the polarization rotation in relaxor ferroelectric $(1-x)PbZn_{1/3}Nb_{2/3} - xPbTiO_3$*, Appl. Phys. Lett. 92 (2008), p. 172911.
[23] I.K. Jeong, C.Y. Park, J.S. Ahn, S. Park, and D.J. Kim, *Ferroelectric-relaxor crossover in $Ba(Ti_{1-x}Zr_x)O_3$ studied using neutron total scattering measurements and reverse Monte Carlo modeling*, Phys. Rev. B 81 (2010), p. 214119.
[24] C. Laulhé, F. Hippert, J. Kreisel, M. Maglione, A. Simon, J.L. Hazemann, and V. Nassif, *EXAFS study of lead-free relaxor ferroelectric $BaTi_{1-x}Zr_xO_3$ at the Zr K-edge*, Phys. Rev. B 74 (2006), p. 014106.
[25] C. Laulhé, F. Hippert, R. Bellissent, A. Simon, and G.J. Cuello, *Local structure in $BaTi_{1-x}Zr_xO_3$ relaxors from neutron pair distribution function analysis*, Phys. Rev. B 79 (2009), p. 064104.
[26] C. Laulhé, A. Pasturel, F. Hippert, and J. Kreisel, *Random local strain effects in homovalentsubstituted relaxor ferroelectrics: A first-principles study of $BaTi_{0.74}Zr_{0.26}O_3$*, Phys. Rev. B 82 (2010), p. 132102.
[27] T. Egami and S.J.L. Billinge, *Underneath the Bragg Peaks – Structural Analysis of Complex Materials*, Pergamon, Oxford, 2003.
[28] J. Ravez and A. Simon, *Temperature and frequency dielectric response of ferroelectric ceramics with composition $Ba(Ti_{1-x}Zr_x)O_3$*, Eur. J. Solid State Inorg. Chem. 34 (1997), pp. 1199–1209.
[29] B. Ravel, E.A. Stern, R.I. Vedrinskii, and V. Kraizman, *Local structure and the phase transition of $BaTiO_3$*, Ferroelectrics 206-207 (1998), pp. 407–430.
[30] G.H. Kwei, A.C. Lawson, S.J.L. Billinge, and S.W. Cheong, *Structure of the ferroelectric phases of barium titanate*, J. Phys. Chem. 97 (1993), pp. 2368–2377.
[31] I. Levin, T.G. Amos, S.M. Bell, L. Farber, T.A. Vanderah, R.S. Roth, and B.H. Toby, *Phase equilibria crystal structures, and dielectric anomaly in the $BaZrO_3$-$CaZrO_3$ system*, J. Solid State Chem. 175 (2003), pp. 170–181.
[32] A.R. Akbarzadeh, I. Kornev, C. Malibert, L. Bellaiche, and J.M. Kiat, *Combined theoretical and experimental study of the low-temperature properties of $BaZrO_3$*, Phys. Rev. B 72 (2005), p. 205104.
[33] D. Haskel, B. Ravel, M. Newville, and E.A. Stern, *Single and multiple scattering XAFS in $BaZrO_3$: A comparison between theory and experiment*, Physica B 208–209 (1995), p. 151.
[34] D.C. Koningsberger and R. Prins, *X-ray Absorption: Principles, Applications, Techniques of EXAFS, SEXAFS and XANES*, John Wiley & Sons, New York, 1988.
[35] A.L. Ankudinov, B. Ravel, J.J. Rehr, and S.D. Conradson, *Real-space multiple-scattering calculation and interpretation of X-ray-absorption near-edge structure*, Phys. Rev. B 58 (1998), pp. 7565–7576.
[36] C. Laulhé, *Structure Locale dans un Ferroélectrique Relaxeur: $BaTi_{1-x}Zr_xO_3$*, Grenoble Institute of Technology, Grenoble, 2007.
[37] M. Newville, B. Ravel, D. Haskel, J.J. Rehr, E.A. Stern, and Y. Yacoby, *Analysis of multiple-scattering XAFS data using theoretical standards*, Physica B 208-209 (1995), pp. 154–156.
[38] A. Frenkel, E.A. Stern, A. Voronel, M. Qian, and M. Newville, *Solving the structure of disordered mixed salts*, Phys. Rev. B 49 (1994), pp. 11662–11674.
[39] R.E. Cohen, *Origin of ferroelectricity in perovskite oxides*, Nature 358 (1992), pp. 136–138.
[40] Y. Liu, R.L. Withers, B. Nguyen, and K. Elliott, *Structurally frustrated polar nanoregions in $BaTiO_3$-based relaxor ferroelectric systems*, Appl. Phys. Lett. 91 (2007), p. 152907.
[41] R. Comès, M. Lambert, and A. Guinier, *The chain structure of $BaTiO_3$ and $KNbO_3$*, Solid State Commun. 6 (1968), pp. 715–719.
[42] R. Comès, M. Lambert, and A. Guinier, *Désordre linéaire dans les cristaux (cas du silicium, du quartz, et des pérovskites ferroélectriques)*, Acta Crystallogr. A 26 (1970), p. 244.